TRANSITION ON SWEPT WINGS

Edward B. White and William S. Saric
Mechanical and Aerospace Engineering, Arizona State University
Tempe, AZ 85287-6106, USA

Abstract

Crossflow-dominated swept-wing transition represents both a fundamentally challenging and a technologically important research problem. The nature of the crossflow instability is such that the boundary-layer flow is subject to strongly non-linear behavior very early in its evolution. Because of this, it has resisted treatment by linear methods, including e^N, and therefore, predicting the transition location for even the simplest configurations is not possible at present. This is in spite of the fact that a very complete understanding of the primary crossflow instability has been developed and exceptionally good agreement between experiments and computations has been obtained. What is lacking is a detailed description of the breakdown phenomenon in the final stages of transition. It is thought that breakdown is caused by the growth of a high-frequency secondary instability. Although there is growing evidence that this is the case, there is still little experimental data. It is the objective of the current work to provide such data on the behavior of the breakdown region. This data, coupled with the existing primary instability model, will be another step towards a complete transition prediction method for swept-wing transition.

1 Introduction

Transition to turbulence in crossflow-dominated, swept-wing boundary layers has received considerable attention over the past 15 years. The reason is the obvious engineering benefit that would result from enabling fully laminar flow for this class of wing. The difficulty faced in confronting this problem has been the strongly nonlinear nature of the crossflow instability. Linear methods have provided almost no useful results and therefore tremendous effort has been given to understanding the nonlinear aspects of the phenomenon. Recent reviews of this effort by the two principal experimental research groups are by Bippes [2, 3] at DLR Göttingen, Reibert and Saric [18], and Saric et al. [22] at Arizona State University. Other related reviews are found in Arnal [1], Kachanov [11], Reshotko [20], Crouch [5], and Herbert [9, 10].

The net result of the previous efforts is a very complete understanding of the primary crossflow instability, including details of the nonlinear saturation of the dominant stationary mode and the growth of harmonics. An important consequence is that a means of transition suppression has been developed by Saric et al. [21] that exploits the nature of the nonlinearities.

What is lacking from the current understanding of the crossflow transition process is detailed information regarding the eventual breakdown to turbulence. This information is needed both so that a predictive model of transition location can be developed and so that the success of the transition suppression experiment can be easily extended to other conditions. It is thought breakdown occurs due to a rapidly growing, high-frequency secondary instability that exists in the distorted velocity field resulting from the primary stationary disturbance. Until this part of the transition process is better understood, it will be difficult to generalize the transition suppression re-

sults.

The transition scenario presented here consists of the idea that turbulence is triggered by a high-frequency secondary instability of the inflectional flow produced by stationary crossflow waves. While the current data do not represent a predictive transition model, they do provide a clear experimental description of breakdown and will be a key component of any such model. The actuator system is an array of pneumatically activated surface roughness elements of a flexible material just aft of the attachment line.

The secondary instability transition scenario is based on previous experimental transition location results as well as new, detailed measurements of secondary instability mode shapes and growth rates. The previous experimental evidence shows that the primary instability serves to establish a base state for the secondary instability, but that the ultimate transition behavior is quite insensitive to the details of the primary instability growth as long as the primary disturbance saturates. Instead, the secondary instability is the driving mechanism of breakdown. Mode shapes and growth rates demonstrate this quite convincingly. Moreover, because breakdown occurs so rapidly after the onset of secondary instability growth, it appears that only a few parameters concerning the instability will be required to produce an effective means of transition prediction that can be extended to other configurations.

2 Transition Scenario

The transition scenario discussed below is based on ongoing work at the Arizona State University Unsteady Wind Tunnel on two swept-wing models. The wing used in previous work is designated the NLF(2)-0415 and the wing in current use is designated the ASU(67)-0315. Both have a 1.83-m chord length, a $45°$ sweep angle, and a pressure minimum at 71% chord. The favorable pressure gradient on the suction side of the wings suppresses streamwise Tollmien–Schlichting disturbances and produces a purely crossflow-dominated boundary layer (see Fig. 1 for the ASU wing pressure distribution). The

ASU(67)-0315 in current use is at a $-3°$ angle of attack and zero lift. This orientation produces strong crossflow but requires relatively simple wall liners to simulate infinite-span flow. Figure 2 is a schematic of the wing installed with the wall liners. Because of the similarities of the wings, experience gained on the old NLF wing is directly applicable to the new ASU wing.

In the boundary-layer transition process for crossflow-dominated swept wings there are a number of regimes that can be identified: receptivity, primary linear instability, nonlinear instability associated with the generation of harmonics and saturation, secondary instability growth, and breakdown. Of these, the primary instability and nonlinear growth regimes are the best understood. Many receptivity details are unknown. However, because of the nature of the nonlinear instability, certain details of the receptivity, especially the effect of roughness amplitude, may not be important. Therefore, the current effort is aimed primarily at understanding the role of the secondary instability in the breakdown to turbulence. However, a brief review of receptivity and the primary instability is necessary to motivate the approach to the secondary instability.

2.1 Receptivity and Primary Instability

Detailed physical receptivity mechanisms for crossflow have not been investigated experimentally. However, work at ASU, especially that of Radeztsky et al. [17] and DLR by Deyhle and Bippes [7], provide a parametric understanding of receptivity. The DLR experiments established that for low levels of freestream turbulence, the transition process is dominated by stationary crossflow waves, while at high disturbance levels, traveling waves dominate because of the larger amplitude unsteady initial conditions. These traveling waves have the tendency to wash out the stationary structure. However, the stationary modes may be the most important practical case because of the low freestream turbulence observed in flight situations.

Surface roughness is the other important crossflow receptivity mechanism. Three con-

figurations have been investigated at ASU in a low-disturbance, stationary-wave-dominated boundary layer prior to the current experiment. These are distributed random roughness, isolated static roughness elements, and spanwise-periodic, static roughness arrays. For random, natural-surface roughness, dramatic transition improvements were obtained by decreasing the average roughness level from $3.3\,\mu m$ rms to $0.1\,\mu m$ rms. For $Re_c = 2.4 \cdot 10^6$, this roughness decrease delayed transition from 48% to 77% chord [17]. The isolated roughness element studies established that stationary crossflow features are generated by particular roughness elements at 1–3% chord near the first neutral point of the crossflow instability, and that the most effective spanwise scale is about one-fourth the most amplified stationary crossflow wavelength ($12\,mm$ for the NLF wing at $Re_c = 2.4 \cdot 10^6$). Roughness arrays were used to generate uniform initial disturbance states for primary instability studies by Reibert et al. [19] and Saric et al. [21].

The primary instability studies that employed spanwise-periodic roughness arrays established a number of crossflow-transition features. First, Reibert et al. [19] showed that primary stationary waves quickly become subject to nonlinear evolution. Nonlinearities are important early because although the stationary disturbances are small, the stationary structures are nearly aligned with the boundary-layer flow, so a particular disturbance velocity acts on a fluid element throughout the boundary layer, producing a large integrated effect. This effect is manifested as a severely distorted mean flow. The distortion results in saturation of the primary wave and growth of harmonics. Saturation appears well before transition. The saturation amplitude appears to be independent of the leading-edge roughness amplitude. As the primary wavenumber disturbance saturates, a rich spectrum of harmonics of the primary are produced, but no subharmonics appear. For 12-mm-wavelength roughness arrays, wavelengths of 12, 6, 4, and 3 mm are observed but 24-mm waves are not. A key feature of this is that any initial disturbance with spectral wavelength content *at or greater than* the most

amplified wavelength will produce strongly amplified waves.

The primary instability region is now very well understood and excellent agreement between the computations of Haynes and Reed [8] and the experiments of Reibert et al. [19] has been achieved. The quality of the agreement suggests that all the features important for the primary instability, including details of the nonlinear effects, are adequately modeled and other crossflow-dominated configurations can be computed with some confidence.

The nature of the crossflow nonlinearities suggested a transition control strategy that was applied successfully in the Saric et al. [21] experiment. Because periodic roughness was never observed to produce a subharmonic response, an 8-mm-wavelength primary wave was produced using artificial roughness at $Re_c = 2.4 \cdot 10^6$. At that Reynolds number, the 12-mm mode is most amplified and dominates transition. The 8-mm wave produced harmonics at 4, 2.7, and 2 mm, but no subharmonic at 16 mm in the more amplified wavelength band. Consequentially, the 8-mm mode grew and decayed without leading to transition. However, because no amplified waves were produced at the most highly amplifying chord locations, there was no organized disturbance field and transition was delayed past 80% chord, exceeding the most highly polished leading-edge transition location. This experiment shows that transition control is possible using a simple, static roughness actuator at the leading edge. What is desired now is a detailed understanding of what conditions lead directly to transition so that the success of the Saric et al. experiment can be generalized to a variety of conditions.

2.2 Secondary Instability and Breakdown

Understanding of the primary instability is now quite complete. However, this has not yielded a predictive model of transition location. The reason appears to be that the primary disturbances are relatively stable once they have saturated. Instead, breakdown to turbulence appears to be

due to a high-frequency secondary instability that grows in the saturated primary-flow boundary layer.

A high-frequency disturbance prior to transition was first observed by Poll [16] and was specifically investigated as a secondary instability and a source of breakdown by Kohama et al. [13]. This experiment included measurements intended to determine the location of the secondary instability mode relative to breakdown patterns observed in naphthalene flow-visualization experiments. Kohama et al. reported that the initiation of turbulent wedges in the naphthalene occurred in doubly inflected streamwise velocity profiles (inflection points in the wall-normal direction) and concluded that the high-frequency fluctuations observed in hotwire measurements acquired away from the wall were at the same span location. However, computations of secondary instability mode shapes by Malik et al. [14] for Falkner–Skan–Cooke flows and Malik et al. [15] for the ASU swept-wing configuration showed quite different behavior. Both of these computational efforts yielded secondary instabilities in the frequency range measured by Kohama et al. [13] (2–3 kHz for the ASU swept wing at $Re_c = 2.66 \cdot 10^6$). However, the computations indicated that the secondary instability mode is located on the opposite side of the stationary vortex structure than Kohama et al. reported.

Given the discrepancy of the experimental and computational efforts, there are two specific objectives of the current work with regard to the secondary instability. The first is to resolve the disagreement regarding the location of the secondary instability mode. The second is to more completely characterize the breakdown process in terms of the secondary instability mode growth. No detailed experiment has yet been conducted regarding the manner in which breakdown occurs. It is hoped that meeting these objectives will not only resolve the disagreement between the previous results but also provide a database from which more general transition parameters may be drawn.

2.3 Secondary Instability Growth Experiment

For this experiment, static leading-edge surface roughness is applied on a 12-mm spacing at 2.5% chord on the ASU(67)-0315 model. Four cases are examined: $Re_c = 2.4 \cdot 10^6$ with 6- and 18-μm roughness and $Re_c = 2.0 \cdot 10^6$ and $Re_c = 2.8 \cdot 10^6$ with 18-μm roughness. Roughness configurations are written as $[k|\lambda]$, where the roughness height, k, is in microns and the wavelength, λ, is in millimeters. At various chord locations, the mean and fluctuating components of the nearly[1] streamwise velocity are obtained for one wavelength of the primary disturbance using a single-element hotwire. A grid of points is acquired at each chord location for a particular structure as it evolves. Typical grid spacings are 1 mm in the span direction (for all cases the primary spanwise wavelength is 12 mm) and 150–300 μm in the wall-normal direction. At each grid point, mean and fluctuating velocity signals are acquired for 1.6 sec. The boundary-layer velocity signal is normalized by the boundary-layer edge velocity. The edge velocity is monitored by a second hot wire in the freestream. The spectrum of the fluctuating velocity disturbances at each point is calculated and a narrow band of these frequencies is used to generate mode shapes for each of the amplified secondary instabilities.

The coordinate system used for these measurements is denoted x, Y, z. The lower-case coordinates, x and z, are the model-oriented coordinates representing chord and span and are measured perpendicular and parallel to the leading edge. The upper-case coordinate, Y, is a global, test-section-oriented distance from the wing surface.

The first case presented is $[6|12]$ at $Re_c = 2.4 \cdot 10^6$. For this case, the mean streamwise flow is significantly distorted by 40% chord. Figure 3 shows contours of the mean streamwise velocity for one wavelength of the primary disturbance. The flow is into the page and the crossflow di-

---

[1]The hotwire is aligned so that the velocity component parallel to the global test-section X axis is acquired. The streamlines are deflected somewhat from this direction.

rection is $-z$ (right to left). Notice that the spanwise velocity gradients are nearly as strong as the wall-normal gradients. For this chord location, naphthalene would remain in a band centered on $z = 94$ mm where the wall shear stress is a minimum. Velocity fluctuation spectra for an array of points at $z = 94$ mm (Fig. 4) indicate two amplified modes: a traveling crossflow mode centered at 200 Hz and the high-frequency secondary instability centered at 3.0 kHz. This is the most-upstream chord location at which the secondary instability is clearly evident for this set of conditions. Integrating the mode energy from 150–250 Hz for the traveling crossflow mode and 2.5–3.5 kHz for the secondary instability provides the mode shapes shown in Figs. 5 and 6, respectively. These figures coincide with the mean flow in Fig. 3 and show both that the primary traveling crossflow mode has a strong spatial periodicity that is fixed relative to the stationary structure. The figures also show that the secondary instability is located *not* in a region centered on the doubly inflected profiles suggested by Kohama et al. [13], but instead on the opposite side of the low-momentum upwelling region, $z < 94$ mm.

Further downstream at 46% chord, the mean streamwise velocity contours are somewhat more distorted (Fig. 7), but now the fluctuations are dramatically increased relative to the levels at 40% chord. Some of the points are clearly turbulent, based on the flattened appearance of the spectra (Fig. 8). At this location, the traveling crossflow mode could not be satisfactorily extracted from the frequency-domain data. The 3.0-kHz secondary instability mode could be extracted, however. The secondary mode shape shown in Fig. 9 is quite similar to the earlier shape. A plot of the total (100 Hz–8.0 kHz bandpass) fluctuation amplitude contours in Fig. 10 reveals that the maximum fluctuation intensities that are associated with the flat, turbulent spectra are originating from the position of the secondary instability mode. Notice that the region that is the most strongly inflectional (in the 2-D boundary-layer sense) at $z = 80$ mm, $Y = 2.75$ mm *is not* an especially active region, and it is certainly not the location of the initiation of breakdown.

This distribution of energy in the secondary instability and in the total fluctuations at the breakdown location explain the pattern observed in naphthalene flow-visualization experiments starting with those of Dagenhart and Saric [6]. The flow visualization experiments show turbulent wedges originating from points on the crossflow side of low-momentum regions. This arrangement is shown schematically in Fig. 11. The explanation for the breakdown initiation at this location lies with the secondary instability mode shape. Breakdown is spatially coincident with secondary instability, and the secondary instability mode is closest to the wall on the crossflow side of the low-momentum upwelling region. A schematic of the key features in the Y, z plane is given in Fig. 12.

Besides being simply an explanation of the flow-visualization breakdown pattern, the mode-shape data have another immediate consequence. It is a possible explanation as to why the Kohama et al. [13] experiment identified the doubly inflected region as the source of breakdown. In that experiment, only single-line scans were performed. Therefore, the authors may have failed to realize the spatial extent of the secondary instability mode, as any particular scan in Y or z would detect only a small portion of the mode. The spatial extent and orientation are important because the secondary instability mode associated with a particular stationary structure may overlap a neighboring structure. This was especially true for Kohmama et al. [13] because the experiment was performed before artificial roughness arrays were used to enforce a uniform initial condition and large spanwise nonuniformities were common. It is now clear that a breakdown location indicated by flow visualization is the result of the secondary mode with a peak that may lie as much as half a primary wavelength away in the span direction.

Yet another consequence of the secondary instability mode shape and breakdown location concerns the use of surface-mounted shear-stress sensors. Surface-mounted transition sensors such as hot-film anemometers will be necessary for transition detection in flight both for experimen-

tal purposes and as part of an eventual active-feedback transition control system. A transition detection scheme using hot films developed by Chapman et al. [4] provides a proper-orthogonal-decomposition (POD) technique useful for unambiguous, quantitative transition detection. The POD identifies chordwise peaks of the primary and secondary disturbance energies. The primary peak is defined as the onset of transition and the secondary peak is defined as the onset of turbulence. The transition position generated by the POD correlates well with the naphthalene-flow-visualization transition front. Key to using this technique, however, is proper location of the surface hot films. The films must be positioned so that the secondary instability is adequately detected. In the Chapman et al. [4] work, this was taken to be at the span location as the doubly inflected streamwise velocity profile. The data presented here indicate that the success of positioning shear-stress sensors at the doubly inflected span position may have been a coincidence based on the particular disturbance wavelength under investigation. If the dominant spanwise wavelength were different, the doubly inflected region and the portion of the secondary instability mode close to the wall might not coincide. Thus the design of a transition detection system must bear in mind the details of the secondary instability mode shape with respect to the stationary structure.

Besides the conclusions that may be drawn from the disturbance mode shapes regarding the nature of breakdown, the growth of the various disturbance modes are also available. In Fig. 13 amplitudes of four modes are presented, normalized by the amplitudes at their initial measurement locations. The stationary ($f = 0$) mode amplitude is computed by obtaining a spanwise root-mean-squared (rms) variation of the mean velocity profiles about the average mean velocity profile. This rms curve is integrated in Y to obtain a stationary mode amplitude. The amplitude of the fluctuating ($f \neq 0$) modes is obtained by integrating over narrow frequency bands at each point, and then over one wavelength of the disturbance. The traveling crossflow wave integration is from 150–250 Hz. Two high-frequency secondary modes are observed, one centered at

3 kHz with an integration bandpass from 2.5–3.5 kHz and another centered at 6 kHz with an integration bandpass from 7.0–8.0 kHz. These high-frequency modes are designated modes I and II, respectively, after the notation adopted by Malik et al. [15].

The growth of the various modes shown in Fig. 13 provides another indication that growth of the secondary instability is the key factor in the breakdown of crossflow boundary layers. From 30–40% chord, the stationary and traveling crossflow modes grow by less than a factor of five and by 40% chord the stationary instability has saturated. However, at 42% chord, the mode I secondary instability undergoes explosive growth followed by mode II at 43% chord. At 46% chord, the first turbulent spectra appear and by 48% chord nearly the entire field is turbulent. Through the last portion of breakdown, the traveling crossflow mode appears to undergo more rapid growth, but this may be an artifact of the quickly spreading spectral peak centered on the mode I secondary instability. That is, the mode amplitude integration from 150 to 250 Hz detects both the contribution of the traveling wave centered at 200 Hz and the tail of the very broad high-amplitude peak at 3 kHz. In any case, it is clear that the secondary instability is driving the breakdown process.

Two of the other experimental cases, $Re_c = 2.4 \cdot 10^6$ and $Re_c = 2.8 \cdot 10^6$ both with [18|12] roughness, demonstrate behavior equivalent to the $Re_c = 2.4 \cdot 10^6$, [6|12] roughness case described above. In the $Re_c = 2.4 \cdot 10^6$, [18|12] case (i.e., same Reynolds number, increased roughness amplitude) the stationary mode saturation level is increased 5% relative to the [6|12] case, but this difference is no greater than typical spanwise variations for a single test at that Reynolds number, even with the use of an artificial roughness array. Saturation is achieved upstream from the low-amplitude-roughness case and transition occurs at 42% chord. Again, the difference is within the range of typical spanwise variations that is observed for a single test. The nearly constant saturation amplitude and transition location agree with the findings of Reibert et al. [19]. In that experiment using the NLF wing, an in-

crease of roughness amplitude from 6–48 µm at $Re_c = 2.4 \cdot 10^6$ only moved the average transition location from 52% to 49% chord.

The $Re_c = 2.8 \cdot 10^6$, $[18|12]$ case shows qualitatively similar behavior. There transition occurred between 34% and 35% chord. The mode I high-frequency secondary instability is at 3.2 kHz and the mode II instability is centered at a frequency greater than 7 kHz. The center frequency appears to be less than 8 kHz, but because the low-pass filter cutoff is at 8 kHz, the location of the peak is not certain. Both the mode I and II instabilities occur over a narrower band than do the instabilities in the $Re_c = 2.4 \cdot 10^6$ cases.

A different type of behavior is observed for the $Re_c = 2.0 \cdot 10^6$, $[18|12]$ case. At this lower Reynolds number, saturation of the primary stationary structure occurs as usual and two broad high-frequency instability modes are observed at 1.5 and 3.0 kHz. However, the high-frequency modes also appear to saturate. Transition *is not* observed via a rapid breakdown originating from the location of the secondary instability modes. Instead, the stationary structure is slowly eroded by high-amplitude, *laminar* fluctuations. For this particular case, some of the primary structures do appear to undergo rapid breakdown and turbulent wedges originating from these points spread across the wing aft to 60% chord. It appears that this particular case of $Re_c = 2.0 \cdot 10^6$, $[18|12]$ roughness represents a boundary in the parameter space governing the breakdown phenomenon and is still being investigated.

3   Conclusions

The current work is intended to provide an improved experimental understanding of the breakdown process and how it is related to the high-frequency secondary instability. To summarize the current experimental results, the high-frequency secondary instability mode appears not in the regions that are doubly inflected but rather on the downstream crossflow side of the low-momentum upwelling region. This suggests that in general, one must use caution applying 2-D experience to such a highly 3-D boundary layer. Streamwise velocity gradients in many directions

through the boundary layer, including the spanwise direction, produce strongly inflectional profiles so the wall-normal profile is not, in all likelihood, the most unstable profile. In a case such as this a whole-field criteria is the most appropriate means of understanding the instability. The location of the secondary instability mode also explains the nature of breakdown patterns observed in naphthalene flow-visualization experiments.

Both the mode shape and growth data presented here show that the secondary instability is indeed the key factor in triggering breakdown of saturated crossflow boundary layers. The four cases discussed do not yet represent a database from which a predictive transition model can be determined for this configuration. However it is clear that such a model will have a strong dependence on the primary stationary mode amplitude and a boundary-layer-scale Reynolds number. It is uncertain at present to what extent other factors such as the amplitude of stationary harmonics and traveling crossflow modes influence the location of breakdown.

The secondary instability data show good qualitative agreement with computations of Malik et al. [15] and confirms some preliminary observations of Kawakami et al. [12] concerning the secondary instability on a swept plate. Improving the agreement between the secondary-instability computations and experiments is important because since there is such good agreement between model and experiment for the primary instability, it may soon be possible to extend the range of the calculations from the linear primary region through the nonlinear region and accurately predict the growth of the secondary instability up to the point of breakdown.

References

[1] Arnal D. Laminar-turbulent transition: Research and applications in France. *AIAA Paper 97-1906*, 1997.

[2] Bippes H. Environmental conditions and transition prediction in 3-D boundary layers. *AIAA Paper 97-1906*, 1997.

[3] Bippes H. Basic experiments on transition in three-dimensional boundary layers dominated by crossflow instability. *Prog. Aero. Sci.*, Vol. 35, No 4, pp 363–412, 1999.

[4] Chapman K. L., Reibert M. S., Saric W. S., and Glauser M. N. Boundary-layer transition detection and structure identification through surface shear-stress measurements. *AIAA Paper 98-0782*, 1998.

[5] Crouch J. D. Transition prediction and control for airplane applications. *AIAA Paper 97-1907*, 1997.

[6] Dagenhart J. R. and Saric W. S. Crossflow stability and transition experiments in swept-wing flow. NASA TP-1999-209344, 1999.

[7] Deyhle H. and Bippes H. Disturbance growth in an unstable three-dimensional boundary layer and its dependence on initial conditions. *J. Fluid Mech.*, Vol. 316, pp 73–113, 1996.

[8] Haynes T. S. and Reed H. L. Simulation of swept-wing vortices using nonlinear parabolized stability equations. *J. Fluid Mech.*, Vol. 405, pp 325–349, 2000.

[9] Herbert Th. On the stability of 3-D boundary layers. *AIAA Paper 97-1961*, 1997.

[10] Herbert Th. Transition prediction and control for airplane applications. *AIAA Paper 97-1908*, 1997.

[11] Kachanov Y. S. Experimental studies of three-dimensional instability of boundary layer. *AIAA Paper 96-1976*, 1996.

[12] Kawakami M., Kohama Y., and Okutsu M. Stability characteristics of stationary crossflow vortices in three-dimensional boundary layer. *AIAA Paper 99-0811*, 1999.

[13] Kohama Y., Saric W. S., and Hoos J. A. A high-frequency, secondary instability of crossflow vortices that leads to transition. *Proc. of the Royal Aero. Soc. Conf. on Boundary-Layer Transition and Control*, 1991.

[14] Malik M. R., Li F., and Chang C. L. Crossflow disturbances in three-dimensional boundary layers: Nonlinear development, wave interaction and secondary instability. *J. Fluid Mech.*, Vol. 268, pp 1–36, 1994.

[15] Malik M. R, Li F., and Chang C. L. Nonlinear crossflow disturbances and secondary instabilities in swept-wing boundary layers. *Proc. IUTAM Symposium on Nonlinear Instability and Transition in Three-Dimensional Boundary Layers*, pp 257–266, 1996.

[16] Poll D. I. A. Some observations of the transition process on the windward face of a long yawed cylinder. *J. Fluid Mech.*, Vol. 150, pp 329–356, 1985.

[17] Radeztsky R. H., Jr., Reibert M. S., and Saric W. S. Effect of isolated micron-sized roughness on transition in swept-wing flows. *AIAA J.*, Vol. 37, No 11, pp 1371–1377, 1999.

[18] Reibert M. S. and Saric W. S. Review of swept-wing transition. *AIAA Paper 97-1816*, 1997.

[19] Reibert M. S., Saric W. S., Carrillo R. B., Jr., and Chapman K. L. Experiments in nonlinear saturation of stationary crossflow vortices in a swept-wing boundary layer. *AIAA Paper 96-0184*, 1996.

[20] Reshotko E. Progress, accomplishments and issues in transition research. *AIAA Paper 97-1815*, 1997.

[21] Saric W. S, Carrillo Jr. R. B, and Reibert M. S. Leading-edge roughness as a transition control mechanism. *AIAA Paper 98-0781*, 1998.

[22] Saric W. S., Carrillo R. B, Jr., and Reibert M. S. Nonlinear stability and transition in 3-D boundary layers. *Meccanica*, Vol. 33, pp 469–487, 1998.
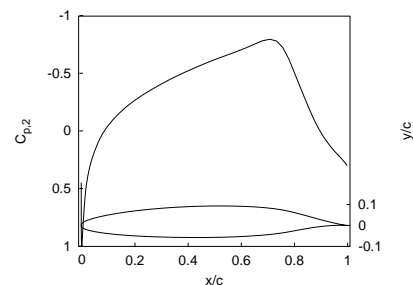
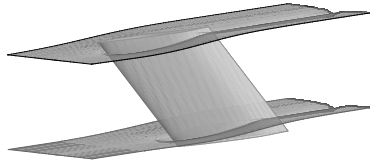**Fig. 1** ASU(67)-0315 suction-side pressure coefficient and contour.

Fig. 2 Schematic of installed wing with wall liners.

Fig. 3 Streamwise mean-flow velocity contours for $Re_c = 2.4 \cdot 10^6$, $x/c = 0.40$, [6|12] roughness. Lines are 10% contours of u/u_e.

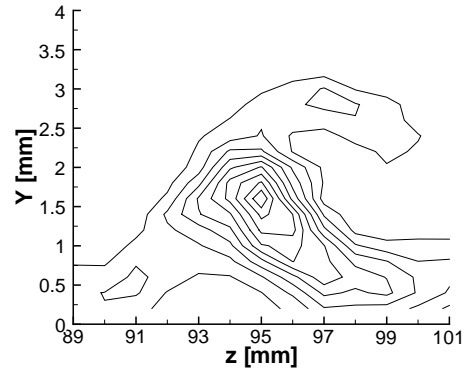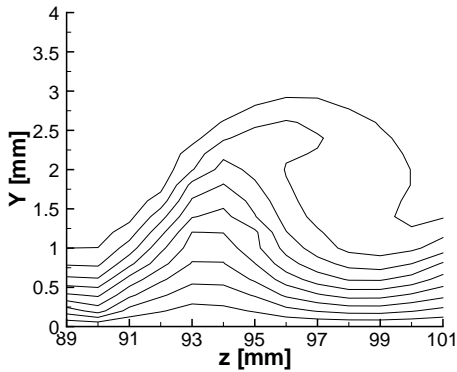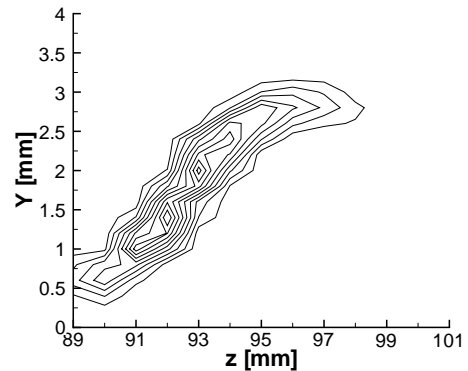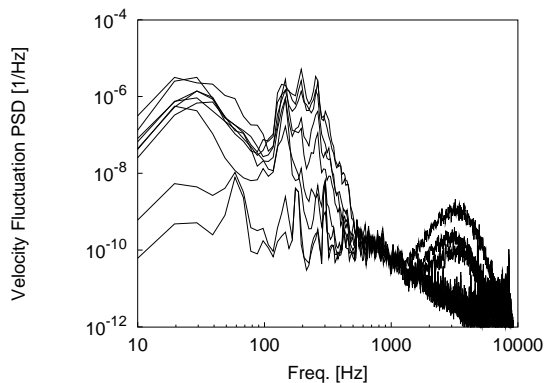**Fig. 4** Fluctuation spectra for $z = 94$ mm in Fig. 3 (100 Hz–8.0 kHz bandpass).

Fig. 5 Rms contours of the traveling crossflow mode shape (150–250 Hz bandpass) for Fig. 3. Lines are 10% contours of the maximum amplitude.
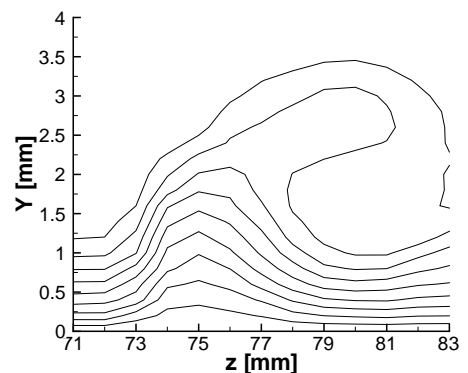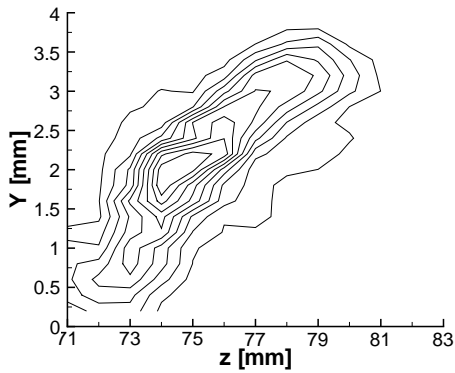
Fig. 6 Rms contours of the secondary instability mode shape (2.5–3.5 kHz bandpass) for Fig. 3. Lines are 10% contours of the maximum amplitude.
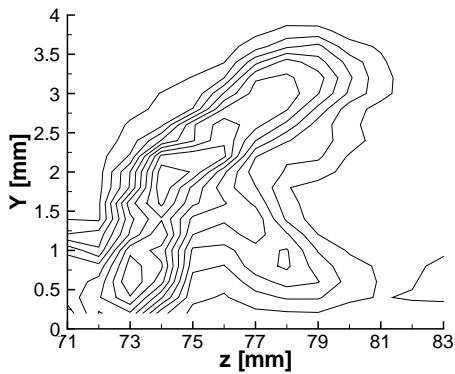
Fig. 7 Mean-flow contours for $Re_c = 2.4 \cdot 10^6$, $x/c = 0.46$, [6|12] roughness. Lines are 10% contours of u/u_e.
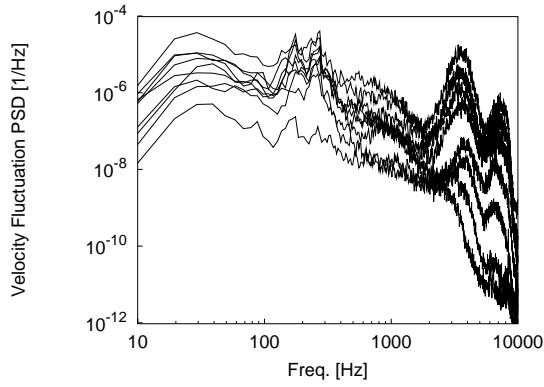
Fig. 8 Fluctuation spectra for $z = 75\,\mathrm{mm}$ in Fig. 7. Spectra are taken at points 0.4, 0.8, ..., 3.6 mm from the wall.

Fig. 11 Schematic of naphthalene flow visualization of breakdown in the x, z plane.

Fig. 9 RMS contours of the secondary instability mode shape (2.5–3.5 kHz bandpass) for Fig. 7. Lines are 10% contours of the maximum amplitude.

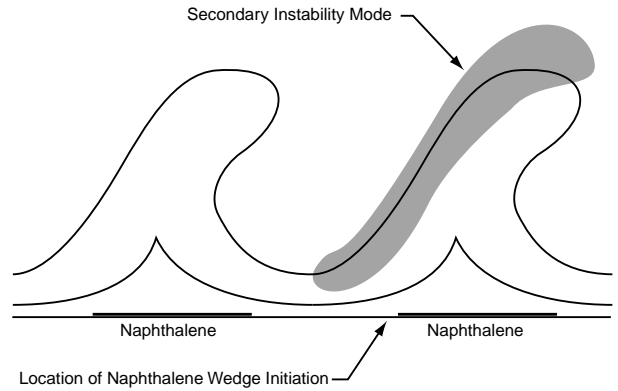**Fig. 12** Schematic of hotwire reconstruction of breakdown in the Y, z plane.

Fig. 10 Total fluctuation contours (100–8000 Hz bandpass) for Fig. 7. Lines are 10% contours of the maximum amplitude.
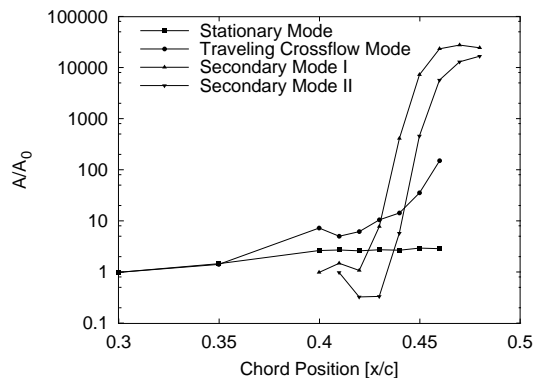

Fig. 13 Mode growth for $Re_c = 2.4 \cdot 10^6$, [6|12] roughness.